A multilayered/sandwich triangular finite element applied to linear and non-linear analyses

O. Polit [a,*], M. Touratier [b]

[a] LMpX-Université Paris X, 1 Chemin Desvallières, 92410 Ville d'Avray, France
[b] LMSP-ENSAM, 151 Bd de l'Hôpital, 75013 Paris, France

In this paper, we focus on the geometrically non-linear behaviour of multilayered plates. For this purpose, a high order plate model is used which exactly ensures both the continuity conditions for displacements and transverse shear stresses at the interfaces between layers of a laminated structure, and the boundary conditions at the upper and lower surfaces of the plates. Furthermore, the transverse shear strain distributions are given by cosine functions and shear correction factors are not needed.

Based on this refined plate model, a six node C^1 conforming triangular finite element is developed using a displacement approach. The Argyris interpolation is used for transverse displacement and the Ganev interpolation is used for membrane displacements and transverse shear rotations. This choice avoids the transverse shear locking problem.

Furthermore, the transverse normal stress can be deduced from equilibrium equations at the post-processing level and a linear variation with respect to the in-plane coordinates is obtained using these high degrees of interpolation polynomia.

A set of linear and non-linear tests is presented in order to show the efficiency of this finite element.

Keywords: C^1 finite element; Multilayered plate; Refined model; Linear analysis; Non-linear analysis; Transverse normal stress

1. Introduction

Multilayered plates and in particular sandwich panels are more and more used in aerospace, automotive and in general industrial structures. Designing this kind of structure is needed and requires the use of complex numerical tools. A recent paper [1] gives an overview of the state of the art concerning sandwich panels and readers are also referred to Reddy's book [2] dedicated to laminated composite plates.

In order to accurately evaluate stresses which are of high importance for multilayered structures, three-dimensional or layer-wise bi-dimensional finite element analysis can be used. The cost of the first approach is very high because a large number of elements are required in the thickness direction, while for the second, the number of unknowns depends on the layer number and almost the same cost as a 3D analysis is reached. From this point of view, the aim of this work is to present an efficient, simple to use and very accurate numerical tool.

This new numerical tool includes transverse shear effects and continuity requirements between layers in order to predict displacements and stresses of such structures for design applications. Another objective is the use of the five conventional generalized displacements in the plate field.

The choice of the finite element method is evident but very few finite elements dedicated to this kind of analysis, including all the above capabilities without numerical problems (shear locking, spurious modes,...), exist in the literature. In fact, it is very difficult to achieve an efficient element including these capabilities for sandwich structure analysis. From the authors' knowledge of recent finite element literature, Sciuva [3] and Carrera [4] developed finite elements taking into account refined shear deformation and interlayer continuity requirements, but those elements exhibit a severe transverse shear locking and need selective or reduced integration techniques. Furthermore, it must be denoted that Carrera finite elements have more than five conventional generalized displacements because two

* Corresponding author. Fax: +33-1-47-09-45-33.
E-mail address: olivier.polit@cva.u-paris10.fr (O. Polit).

"zig-zag" functions are added to the Reissner–Mindlin (RM) model.

In this paper, we present a new C^1 plate finite element based on the refined kinematic model given in [5] and incorporating

- transverse shear strains with a cosine distribution;
- the continuity conditions between layers of the laminate for both displacements and transverse shear stresses;
- the satisfaction of the boundary conditions at the top and bottom surfaces of the plates;
- only five independent generalized displacements (three translations and two rotations) without shear correction factors.

The element is of triangular shape and the generalized displacements are approximated by higher-order polynomia based on the

- Argyris et al. [6] interpolation for the transverse normal displacement;
- Ganev and Dimitrov [7] interpolation for both membrane displacements and transverse shear rotations.

The transverse normal stress is deduced from the equilibrium equations since the finite element is based on high degree interpolation functions. A linear variation of the transverse normal stress with respect to the in-plane coordinates is then obtained.

Furthermore, geometric non-linear effects are included via the Von Karmann assumptions which allow moderately large transverse displacements, while rotations and strains are small.

Some linear static tests are presented and show that the element has a good behaviour and, even with a coarse mesh, gives accurate computations for displacements and stresses compared to the exact three-dimensional elasticity solutions for multilayered plates. Next, we focus our attention on non-linear static and post-buckling tests for sandwich plates with different skins by core material property ratios or angle ply laminates for which few results are available in the literature.

The first part of this paper deals with the multilayered plate model while the second part concerns the finite element development. The last section is dedicated to numerical evaluations.

2. The displacement field assuring interlayer continuity

Let $(x_1, x_2, x_3 = z)$ denote the cartesian co-ordinates so that x_1 and x_2 are in the midplane $(z = 0)$ of a plate of constant thickness e, while z is the transverse normal co-ordinate and t is the time. $u_i^{(k)}(x_1, x_2, z, t),\ i \in \{1, 2, 3\}$ are the cartesian components of the displacement field for the kth layer of a multilayered plate, and the transverse normal strain denoted by ϵ_{33} is negligible, according to the moderately thick plate hypothesis. The material behaviour is admitted linearly elastic and strains and stresses are respectively denoted by $\epsilon_{ij}^{(k)}$ and $\sigma_{ij}^{(k)}$ for the kth layer.

From [8], we assume the following distribution of transverse shear stresses in the kth layer for a plate which may be nonsymmetric and having angle ply layers

$$\begin{aligned}
&\sigma_{13}^{(k)}(x_1, x_2, z, t) \\
&\quad = \left(\bar{C}_{55}^{(k)}\left(f'(z) - \frac{e}{\pi} b_{55} f''(z)\right) + a_{55}^{(k)}\right)\gamma_1^0(x_1, x_2, t) \\
&\qquad + \left(\bar{C}_{45}^{(k)}\left(f'(z) - \frac{e}{\pi} b_{44} f''(z)\right) + a_{54}^{(k)}\right)\gamma_2^0(x_1, x_2, t), \\
&\sigma_{23}^{(k)}(x_1, x_2, z, t) \\
&\quad = \left(\bar{C}_{45}^{(k)}\left(f'(z) - \frac{e}{\pi} b_{55} f''(z)\right) + a_{45}^{(k)}\right)\gamma_1^0(x_1, x_2, t) \\
&\qquad + \left(\bar{C}_{44}^{(k)}\left(f'(z) - \frac{e}{\pi} b_{44} f''(z)\right) + a_{44}^{(k)}\right)\gamma_2^0(x_1, x_2, t),
\end{aligned} \tag{1}$$

where $f(z) = \frac{e}{\pi}\sin\frac{\pi z}{e}$ and $f'(z) = \mathrm{d}f(z)/\mathrm{d}z$; γ_1^0 and γ_2^0 are the transverse shear strains at $z = 0$; $\bar{C}_{ij}^{(k)}$ are the moduli of the material for the kth layer taking into account the zero transverse normal stress hypothesis. The linear elastic constitutive law is expressed as

$$[\sigma^{(k)}] = [\bar{C}^{(k)}][\epsilon^{(k)}]$$

$$\text{with} \begin{cases} \bar{C}_{ij}^{(k)} = C_{ij}^{(k)} - \frac{C_{i3}^{(k)} C_{j3}^{(k)}}{C_3^{(k)}}, & i, j = 1, 2, 6, \\ \bar{C}_{ij}^{(k)} = C_{ij}^{(k)}, & i, j = 4, 5. \end{cases} \tag{2}$$

In Eq. (2), $C_{ij}^{(k)}$ are the three-dimensional moduli of the material for the kth layer, and Eqs. (1) and (2) account for layers having orthotropic axes oriented at various angles with respect to the plate axes.

Otherwise, $\epsilon_{33} = 0$ allows to write down $u_3^{(k)}(x_1, x_2, z, t) = u_3(x_1, x_2, z, t) = v_3(x_1, x_2, t)$. From the definition of the strains, we then have for the transverse shear strains

$$2\epsilon_{\beta 3}^{(k)}(x_1, x_2, z, t) = v_3(x_1, x_2, t)_{,\beta} + u_\beta^{(k)}(x_1, x_2, z, t)_{,3}, \tag{3}$$

where Greek indices $(\alpha, \beta, \ldots)$ take their values in the set $\{1, 2\}$ (Latin ones $(i, j, k, \ldots)$ run from 1 to 3) and $p_{,\alpha} = \partial p/\partial x_a$.

From (2), the transverse shear strains may also be written under the following form:

$$\begin{aligned}
2\epsilon_{13}^{(k)} &= S_{55}^{(k)}\sigma_{13}^{(k)} + S_{45}^{(k)}\sigma_{23}^{(k)}, \\
2\epsilon_{23}^{(k)} &= S_{45}^{(k)}\sigma_{13}^{(k)} + S_{44}^{(k)}\sigma_{23}^{(k)},
\end{aligned} \tag{4}$$

where $[S^{(k)}] = [\bar{C}^{(k)}]^{-1}$ are the material compliances.

Substituting (1) into (4), then equating (3) and (4), and performing an integration with respect to the z co-ordinate, it follows that (when superimposing membrane displacements v_α and denoting θ_α as the true rotations):

$$
\begin{aligned}
u_1^{(k)} &= v_1 - z v_{3,1} + \left(f_1 + g_1^{(k)}\right)(v_{3,1} + \theta_2) \\
&\quad + g_2^{(k)}(v_{3,2} - \theta_1), \\
u_2^{(k)} &= v_2 - z v_{3,2} + g_3^{(k)}(v_{3,1} + \theta_2) \\
&\quad + \left(f_2 + g_4^{(k)}\right)(v_{3,2} - \theta_1), \\
u_3 &= v_3.
\end{aligned} \tag{5}
$$

Functions $f_1, f_2, g_1^{(k)}, \ldots, g_4^{(k)}$ are immediately deduced from Eq. (1) and the above integration performed with respect to the z co-ordinate. These coefficients are determined from the boundary conditions at the top and bottom surfaces of the plate, and from the continuity requirements at the layer interfaces for displacements and stresses, see Béakou and Touratier [8]. Hereafter the superscript (k) for $u_\alpha^{(k)}$ components is omitted in order to lighten the finite element description of the model.

3. Virtual power principle for geometrically non-linear analysis

Let us consider a total Lagrangian configuration and a multilayered plate for which the volume is denoted $V(0)$ and the frontier $S(0)$ where (0) indicates the initial (fixed) configuration used. The boundary value problem is formulated by the following total Lagrangian functional:

$$
\begin{aligned}
J(u, u^*)_{V(0)} &= a(u, u^*)_{V(0)} - f(u^*)_{V(0)} - F(u^*)_{S(0)} \\
&= 0 \quad \forall u^*,
\end{aligned} \tag{6}
$$

where u is the displacement field given above by Eq. (5) and u^* is the virtual velocity field.

The bilinear function a specifies the virtual internal power and the linear functions f and F represent body (including inertia terms) and surface loads.

Expression (6) is nonlinear with respect to displacements (see Eqs. (10) and (11)) and a standard linearization procedure must be used. Without followed forces, the linearized form of Eq. (6) gives

$$
\begin{aligned}
D_u a(\overline{u}, u^*)_{V(0)} \cdot \Delta u &= -a(\overline{u}, u^*)_{V(0)} + f(u^*)_{V(0)} \\
&\quad + F(u^*)_{S(0)},
\end{aligned} \tag{7}
$$

where $u = \overline{u} + \Delta u$, and $\overline{u}$ refers to a known state.

The tangent operator is given by the left member of Eq. (7) while the right member first term depends on the known state.

4. Finite element approximations

In order to use bidimensional finite element approximations, a triangulation of the middle plane of the volume $V(0)$ is considered and we denote Ω_e an elementary domain of the discretization. The superscript h is added and means finite element approximation.

This elementary domain is of triangular shape and only three nodes are used for the geometric approximation.

From the displacement field u given by Eq. (5), a conforming finite element method involves the use of a C^1 finite element approximation for the deflexion v_3^h which belongs to the Sobolev space $H^2(\Omega_e)$. The Argyris interpolation is chosen, see Bernadou [9] or the original paper [6] for more details. Moreover, only a C^0 continuity is required for the membrane displacements v_α^h and the shear rotations θ_α^h. In order to avoid the transverse shear locking which appears when thin plates are modelized [10], the Ganev interpolation [7,9] is used. With these choices, the field compatibility [10] is automatically ensured for the transverse shear strains because Argyris interpolation is a fifth order polynomia and Ganev interpolation is a fourth order polynomia.

The finite element constructed with these interpolations has the following set of degrees of freedom:

- at the corner node, we have the following degrees of freedom:

$$
\begin{array}{cccccc}
v_1 & v_{1,1} & v_{1,2} & v_2 & v_{2,1} & v_{2,2} \\
v_3 & v_{3,1} & v_{3,2} & v_{3,11} & v_{3,22} & v_{3,12} \\
\theta_1 & \theta_{1,1} & \theta_{1,2} & \theta_2 & \theta_{2,1} & \theta_{2,2}
\end{array} \tag{8}
$$

- while, at the mid-side node, they are:

$$
\begin{array}{cccc}
v_1 & v_{1,n} & v_2 & v_{2,n} \\
v_{3,n} & & & \\
\theta_1 & \theta_{1,n} & \theta_2 & \theta_{2,n}
\end{array} \tag{9}
$$

where $p_{,n}$ is the derivative with respect to the normal direction of the edge.

5. The elementary matrices

The finite element procedure must be introduced in Eq. (7) in order to obtain all the elementary matrices.

Strains and virtual strain rates can be split into their linear (index L) and non-linear (index NL) parts as follows:

$$
\begin{aligned}
\left[\epsilon_e^{*h}\right] &= \left[\epsilon_{L_e^h}^*\right] + \left[\epsilon_{NL_e^h}^*\right], \\
\left[\epsilon_e^h\right] &= \left[\epsilon_{L_e^h}\right] + \left[\epsilon_{NL_e^h}\right],
\end{aligned} \tag{10}
$$

where the linear part is classic and the non-linear part, associated with the Von-Karmann assumptions, is given by

$$
\begin{aligned}
\left[\epsilon_{NL_e^h}^*\right]^{\mathrm{T}} &= \Big[v_{3,\,1}^h \; v_{3,\,1}^{*h} \; v_{3,\,2}^h \; v_{3,\,2}^{*h} \; v_{3,\,1}^h \; v_{3,\,2}^{*h} \\
&\quad + v_{3,\,2}^h \; v_{3,\,1}^{*h} \; 0 \; 0 \; 0\Big], \\
\left[\epsilon_{NL_e^h}\right]^{\mathrm{T}} &= \Big[\tfrac{1}{2} v_{3,\,2}^h \; \tfrac{1}{2} v_{3,\,2}^h \; v_{3,\,1}^h \; v_{3,\,2}^h \; 0 \; 0 \; 0\Big].
\end{aligned} \tag{11}
$$

Restriction of Eq. (7) on Ω_e gives for the first term of the right member

$$a(\bar{u}^h, u^{*h})_{\Omega_e} = \int_{\Omega_e} \int_{-e/2}^{e/2} \left[\epsilon_e^{*h}\right]^T \left[\bar{C}^{(k)}\right] \left[\epsilon_e^h\right] dz\, d\Omega_e$$
$$= \int_{\Omega_e} \left[E_e^{*h}\right]^T [A_e] \left[\bar{E}_e^h\right] d\Omega_e + \int_{\Omega_e} \left[E_e^{*h}\right]^T \left[B_e(\bar{u}^h)\right] d\Omega_e, \quad (12)$$

where $[E_e^h]$ (respectively $[E_e^{*h}]$) may be seen as a vector of generalized strains (resp. virtual strain rates), given by

$$\left[E_e^h\right]^T = \Big[v_1^h{}_{,1}\ v_1^h{}_{,2}\ \vdots v_2^h{}_{,1}\ v_2^h{}_{,2}\ \vdots v_3^h{}_{,1}\ v_3^h{}_{,2}\ v_3^h{}_{,11}\ v_3^h{}_{,12}\ v_3^h{}_{,22}$$
$$\vdots \theta_1^h \theta_1^h{}_{,1}\ \theta_1^h{}_{,2} \vdots \theta_2^h \theta_2^h{}_{,1}\ \theta_2^h{}_{,2}\Big]. \quad (13)$$

Matrices $[A_e]$, $[B_e(\bar{u}^h)]$ are the integration with respect to the thickness of the material behaviour which corresponds respectively to: the classical linear part, and the contribution of the non-linear terms depending on the known state $\bar{u}^h$.

The above finite element approximations and the degrees of freedom (dof) vector $[Q_e]$ are introduced in $[E_e^h]^T$ and $[E_e^{*h}]^T$ and allow defining

- the elementary stiffness matrix $[K_e]$

$$\left[Q_e^*\right]^T [K_e] [Q_e] = \int_{\Omega_e} \left[E_e^{*h}\right]^T [A_e] \left[E_e^h\right] d\Omega_e, \quad (14)$$

- the elementary vector (contribution of the non-linear terms) $[L_e(\bar{u}^h)]$

$$\left[Q_e^*\right]^T \left[L_e(\bar{u}^h)\right] = \int_{\Omega_e} \left[E_e^{*h}\right]^T \left[B_e(\bar{u}^h)\right] d\Omega_e. \quad (15)$$

In the same way, the left member of Eq. (7) becomes

$$D_u a(\bar{u}^h, u^{*h})_{\Omega_e(0)} \cdot \Delta u^h$$
$$= \int_{\Omega_e(0)} \left[E_e^{*h}\right]^T [A_e] \left[\Delta E_e^h\right] d\Omega_e(0) + \int_{\Omega_e(0)} \left[E_e^{*h}\right]^T \left[A_e(\bar{u}^h)\right] \left[\Delta E_e^h\right] d\Omega_e(0) + \int_{\Omega_e(0)} \left[E_e^{*h}\right]^T \left[A_e(\bar{\sigma}^h)\right] \left[\Delta E_e^h\right] d\Omega_e(0), \quad (16)$$

where $[\Delta E_e^h]$ stands for the incremental generalized strain vector. The matrix $[A_e(\bar{u}^h)]$ depends on material properties and on both linear and quadratic known state $\bar{u}^h$ while $[A_e(\bar{\sigma}^h)]$ depends on the in-plane stresses.

Finally, the elementary tangent stiffness matrix is given by

$$[K_{Te}(\bar{u}^h)] = [K_e] + [K_e(\bar{u}^h)] + [K_e(\bar{\sigma}^h)], \quad (17)$$

where $[K_e]$ is defined above and

$$\left[Q_e^*\right]^T \left[K_e(\bar{u}^h)\right] [\Delta Q_e] = \int_{\Omega_e(0)} \left[E_e^{*h}\right]^T \left[A_e(\bar{u}^h)\right] \left[\Delta E_e^h\right] d\Omega_e(0), \quad (18)$$

$$\left[Q_e^*\right]^T \left[K_e(\bar{\sigma}^h)\right] [\Delta Q_e] = \int_{\Omega_e(0)} \left[E_e^{*h}\right]^T \left[A_e(\bar{\sigma}^h)\right] \left[\Delta E_e^h\right] d\Omega_e(0). \quad (19)$$

The other terms in the right member of Eq. (7) allow to define the load vector, denoted by $[B_e]$, and the mass matrix, denoted by $[M_e]$, which are classic.

6. The numerical results

The governing matrix equations for the numerical analysis are the following:

Linear static. $[K][Q] = [B]$.

Free vibration. $([K] - \omega^2[M]) = [0]$ which is an eigenvalue problem.

Linearized buckling values. $([K] + \lambda[K(\bar{\sigma}^h)]) = [0]$, an eigenvalue problem where $\bar{\sigma}^h$ is an initial in-plane load and λ is the linearized critical buckling load.

Non-linear static analysis. $[K_T([\bar{Q}])][\Delta Q] = [B] - [K][\bar{Q}] - [L([\bar{Q}])]$ which is solved using a Newton–Raphson scheme based on an incremental force approach.

Post-buckling analysis. $[K_T([\bar{Q}])][\Delta Q] = [B] - [K][\bar{Q}] - [L([\bar{Q}])]$ where a transverse load is first applied in order to introduce a geometric imperfection, and secondly the in-plane load is solved as above.

In this section, different kinematic models are evaluated. The finite element approximations are denoted GAG (for Ganev–Argyris–Ganev) and the following models are compared:

- Sinus model with continuity (SIN-C).
- Kirchhoff–Love model (KL) deduced from (5) with $f_1(z) = f_2(z) = 0;\ g_i^{(k)}(z) = 0$.
- Reissner–Mindlin (RM) model obtained from (5) with $f_1(z) = f_2(z) = z;\ g_i^{(k)}(z) = 0$.

Results based on a C^0 finite element [10] are also presented. This finite element, denoted CL8, has eight nodes and is based on the RM model. It is free of transverse shear locking and has very good convergence and accuracy properties in the field of C^0 finite elements.

It must be denoted that all units used in this section refer to those of the International System (M, K, S, A).

6.1. Linear analysis

The first linear problem considered here was defined by Srinivas and Rao [11] who gives exact three-dimensional elasticity solutions. A simply supported sandwich square plate with a skin by core property ratio β under an uniform transverse load is considered.

The core properties are:

$$E_1 = 897,949, \quad E_2 = 471,424, \quad G_{12} = 262,931,$$
$$G_{13} = 159,914, \quad G_{23} = 266,810, \quad v_{12} = 0.44.$$

The sandwich plate is symmetric and has a skin thickness $e_s = 0.01$, a core thickness $e_c = 0.08$ and a length to thickness ratio of $a/e = 10$.

Table 1 gives results for all the finite elements described above in comparison with the exact three-dimensional elasticity solution. Deflexion v_3 and stresses $\sigma_{11}, \sigma_{22}, \sigma_{13}$, following four kinds of meshes ($N = 1$, 2, 4, 8) in a quarter of the plate are compared. All these meshes are regular and $N = 2$ means that the edges are divided in 2: this mesh contains 4 quadrilaterals or 8 triangles. For the present element GAG/SIN-C, the mesh $N = 2$ gives converged values for both transverse displacement and stresses, including the transverse shear stress. This last value presents a deviation smaller than 4% with respect to the three-dimensional elasticity solution. This table also shows convergence and accuracy information for the other models. Some remarks can be made

- GAG finite element has very fast convergence properties for displacement and stresses;
- CL8 and GAG/RM give the same values for displacement and in-plane stresses but only 200 dof ($N = 2$) are necessary for GAG/RM while 960 dof ($N = 8$) must be used to reach converged values with CL8;
- CL8 and GAG/RM give accurate transverse displacements but cannot give reference values for in-plane and transverse shear stresses;
- GAG/KL clearly indicates that the KL model is not suitable for multilayered panel analysis.

Table 1
Simply supported square sandwich plate under a uniform transverse static pressure

N	dof	$v_3 C_{11}/f_3$	σ_{11}/f_3	σ_{22}/f_3	σ_{13}/f_3
GAG/SIN-C: Sinus model with continuity					
1	55	122.10	66.626	46.337	4.137
2	200	121.88	66.570	46.532	4.104
4	760	121.88	66.742	46.581	4.084
8	2960	121.88	66.748	46.586	4.083
GAG/KL: Kirchhoff–Love model					
1	33	81.746	66.607	39.688	0.
2	120	81.801	69.033	41.353	0.
4	456	81.802	69.125	41.404	0.
8	1776	81.802	69.134	41.410	0.
GAG/RM: Reissner–Mindlin model					
1	55	122.21	62.715	44.680	3.022
2	200	121.95	63.553	45.272	3.033
4	760	121.97	63.650	45.310	3.033
8	2960	121.97	63.650	45.312	3.033
CL8: C^0 eight node finite element					
1	15	117.14	29.134	22.798	1.484
2	60	121.73	56.722	40.993	2.441
4	240	121.96	61.764	44.126	3.026
8	960	121.97	63.179	45.014	3.330
16	3840	121.97	63.678	45.324	3.638
Ref. values [11]		121.72	66.787	46.424	3.964

Convergence properties and accuracy, for different plate models, in comparison with the exact three-dimensional elasticity solution.

Figs. 1–3 give distributions of stress components with respect to the thickness co-ordinate z. Comparison is given between reference values [11] and the Sinus model taking into account continuity or not. For σ_{11} in Fig. 1, distributions with respect to the normal co-ordinate are the same. In Fig. 2 we can observe the contribution of the continuity conditions because σ_{13} must be continuous at the layer interfaces and reference value and GAG/SIN-C have the same distribution. Finally, Fig. 3 presents the σ_{33} values deduced from the equilibrium equations at the post-processing level. Both models, with or without the continuity conditions, give good distributions. The load value is recovered at the top

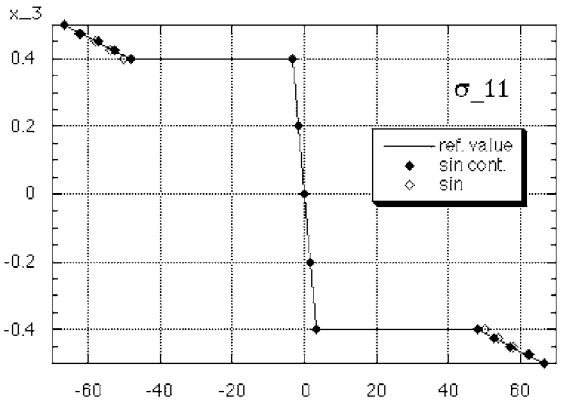

Fig. 1. Distribution of $\sigma_{11}(a/2, a/2, z)$ with respect to the thickness co-ordinate.

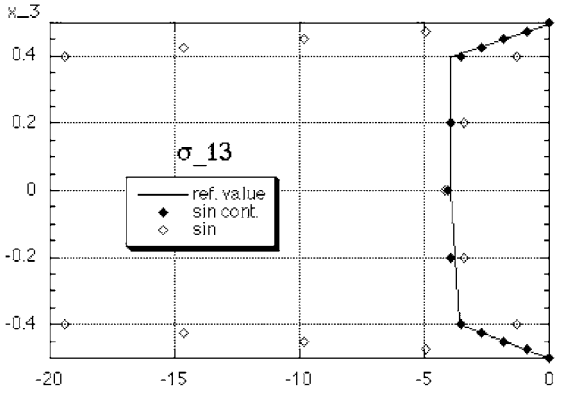

Fig. 2. Distribution of $\sigma_{13}(0, a/2, z)$ with respect to the thickness co-ordinate.

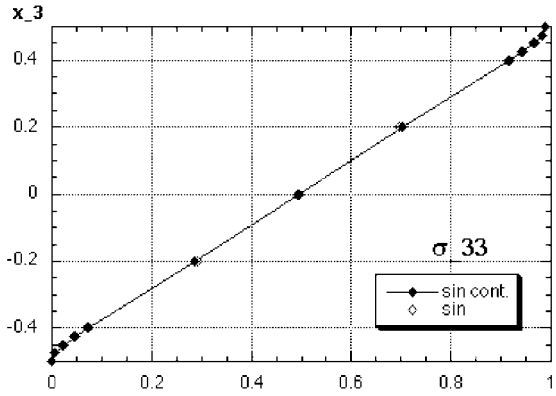

Fig. 3. Distribution of $\sigma_{33}(a/2, a/2, z)$ with respect to the thickness co-ordinate.

surface while zero value is found at the bottom surface, in agreement with the free surface boundary condition.

Some results are given in Table 2 for free vibrations and linear critical buckling loads of the same sandwich panels with a different skin by core property ratios. For the free vibrations, very accurate results are obtained with $N = 1$ mesh with respect to the three-dimensional reference values, while mesh $N = 2$ is necessary to reach converged values for the critical buckling loads. The linear critical buckling loads are slightly overestimated and a deviation smaller than 3.6% is found with respect to the reference values.

6.2. Non-linear analysis

The first set of tests concerns a simply supported square sandwich plate under an uniform transverse load. Properties as above are considered and the study concerns the skin by core property ratio β which varies from 5 to 50. A quarter of the panel is discretized using $N = 2$ mesh.

The load is increased and non-linear equations are solved using a Newton–Raphson algorithm until the results converge within the specific tolerance limit of less than 1% on the displacement increment.

Table 2
Free vibrations and critical buckling loads

N	dof	$\beta = 5$	$\beta = 10$	$\beta = 15$
Free vibrations: $\bar{\omega} = \omega\sqrt{\rho e/C_{11}}$				
1	55	.07714	.09810	.11202
2	200	.07714	.09810	.11202
4	760	.07714	.09810	.11202
Ref. values [11]		.07715	.09810	.11203
Critical buckling loads: $k_{11} = 12\lambda b^2/(\pi A_{11} e^2)$				
1	55	4.167	4.317	4.134
2	200	4.193	4.345	4.163
4	760	4.193	4.345	4.163
Ref. values [11]		4.046	4.200	4.037

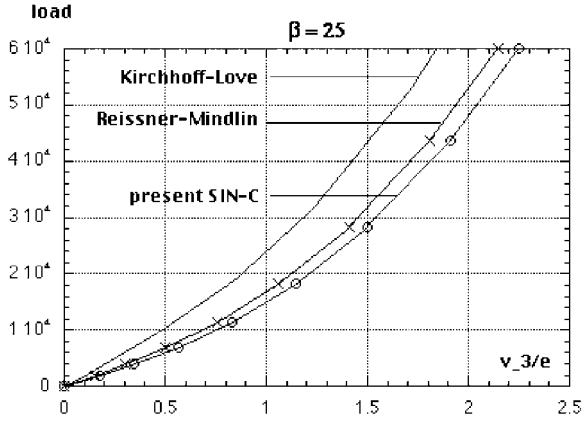

Fig. 4. Transverse displacement $v_3(a/2, a/2, 0)$ of a simply supported square sandwich plate with $\beta = 25$: comparison of different plate models.

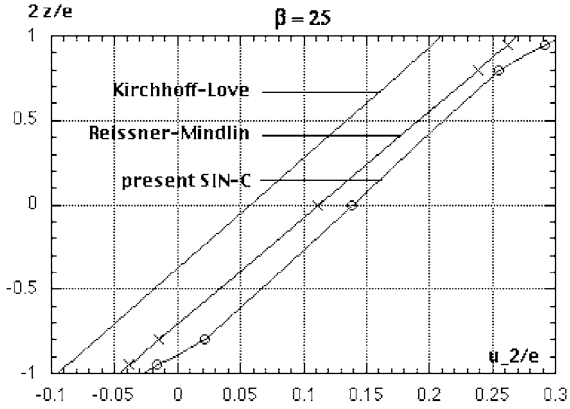

Fig. 5. In-plane displacement $v_2(a/2, 0, z)$ of a simply supported square sandwich panel with $\beta = 25$: comparison of different plate models.

Figs. 4 and 5 give results for $\beta = 25$ and compare the finite elements GAG/KL, GAG/RM, and the present GAG/SIN-C. These figures respectively show the transverse displacement $v_3(a/2, a/2, 0)$ and the in-plane displacement $u_2(a/2, 0, z)$ distributions with respect to the thickness co-ordinate z. In those figures, one can observe the part of the transverse shear stresses and the effect of the assumptions: no transverse shear stresses for the KL model, a constant value in each layer without continuity for the Reissner–Mindlin model and a physical distribution and continuity for the present model.

For different values of β, the transverse displacement $v_3(a/2, a/2, 0)$ is presented in Fig. 6 for linear (curves without marker) and non-linear (curves with markers) analyses. The difference between linear and non-linear results increases significantly when the displacement value increases. It must also be denoted that the higher β is, more the non-linear effect must be taken into account early: for $\beta = 5$, transverse displacement values become significantly different between linear and non-linear an-

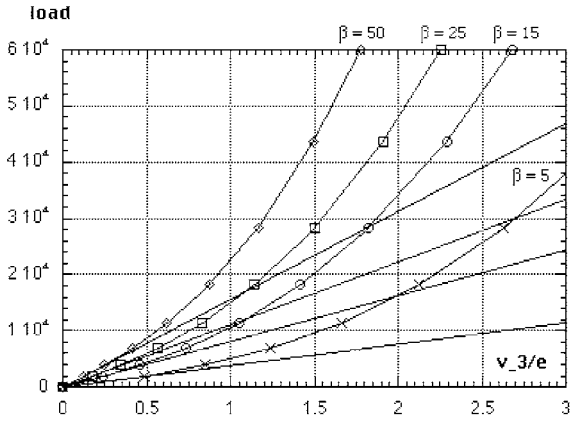

Fig. 6. Simply supported square sandwich plate: influence of β on the transverse displacement $v_3(a/2, a/2, 0)$.

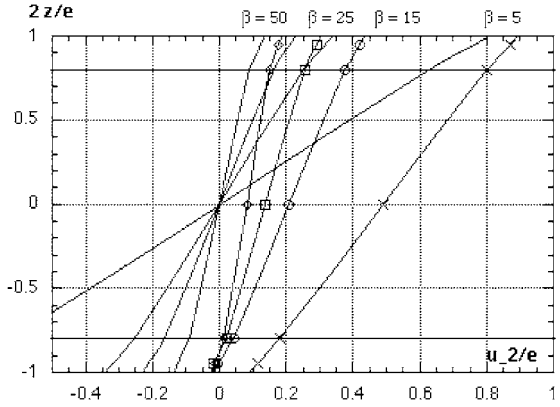

Fig. 7. Simply supported square sandwich plate: influence of β on the in-plane displacement $v_2(a/2, 0, z)$.

alyses for $v_3/e \sim 0.7$ while in the case of $\beta = 50$, it is for $v_3/e \sim 0.4$.

Fig. 7 shows the in-plane displacement $u_2(a/2, 0, z)$ with respect to the thickness co-ordinate for a normal transverse load value of $F_3 = 2 \cdot e4$. Linear (curves without marker) and non-linear (curves with markers) analyses can be compared and $u_2(a/2, 0, 0) = 0$ is satisfied for all β value in the linear cases. The difference is obvious between these two analyses and is more significant for a small rigidity ratio. When the rigidity ratio increases, in-plane displacement decreases. In the case of the non-linear analysis, the in-plane displacement values $u_2(0, a/2, -e/2)$ at the bottom surface are closed to zero, except for $\beta = 5$.

6.3. Buckling and post-buckling analyses

The second set of tests is about buckling and post-buckling analyses. Four layers $(\theta, -\theta, -\theta, \theta)$ simply supported square plate under uniaxial and biaxial in-plane loads are considered. The mesh $N = 2$ is used to model the whole plate.

Material properties are taken from [12] and are given by

$$E_1 = 25 \times 10^9, \quad E_2 = 10^9, \quad G_{12} = 0.5 \times 10^9,$$
$$G_{13} = 0.5 \times 10^9, \quad G_{23} = 0.2 \times 10^9, \quad \nu_{12} = 0.25.$$

All the layers are of equal thickness and we choose $a/e = 10$.

A biaxial load (in N/m) is considered along x_1 and x_2, defined by

- $F_1(0, x_2, 0) = c$ and $F_1(a, x_2, 0) = -c$ with respect to the x_1 co-ordinate.
- $F_2(x_1, 0, 0) = c$ and $F_2(x_1, a, 0) = -c$ along x_2.

Fig. 8 compares the buckling load value for different θ values in the case of a biaxial in-plane load for the three plate models and the effect of the transverse shear stresses is obvious. The KL model overestimates the critical buckling load and the Reissner–Mindlin model lightly overestimates it too. For this latter model, a deviation of 17% with respect to the Sinus model with continuity for $\theta = 45°$ layer orientation is observed.

Finally, post-buckling results are given in Fig. 9 with respect to the layer orientation. The transverse displacement at the plate center is shown versus the in-plane load value. A small uniform transverse load is applied in order to initiate the buckling mode, and then the in-plane load is increased using a Newton–Raphson algorithm until convergence. Linear critical buckling load values presented in Fig. 8, are recovered: the less critical buckling load value is obtained for the homogeneous case, while the higher value is found for a layer orientation of $\theta = 30°$. From the post-buckling curves and for $\theta = 45°$, one can observe that the plate stiffness has the greatest value, as the transverse displacement is smaller for a given load. On the other hand and for the homogeneous case, the slope of the post-buckling curve is nearly horizontal.

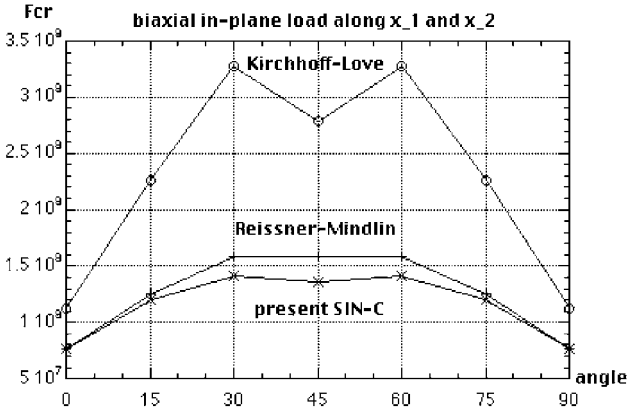

Fig. 8. Four layer $(\theta - \theta)_S$ simply supported square panel under biaxial in-plane load: angle orientation and buckling load values.

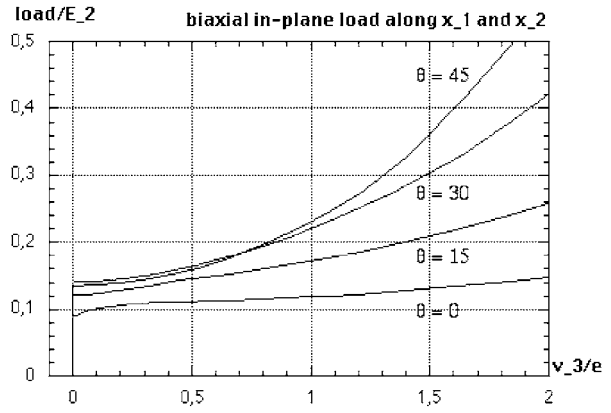

Fig. 9. Four layer $(\theta, -\theta)_S$ simply supported square panel under biaxial in-plane load: angle orientation and post-buckling response.

7. Conclusions and perspectives

A new finite element for the multilayered plate analysis has been presented in this paper. Evaluations for linear and non-linear tests give results in great agreement with available solutions for displacements and stresses and very good convergence and accuracy properties have been demonstrated.

This new finite element is based on a refined kinematic model, including a cosine distribution of the transverse shear strains, the continuity conditions between layers for both displacements and transverse shear stresses, and the satisfaction of the boundary conditions at the top and bottom surfaces of the plate. Furthermore, higher order polynomia are used in order to define the finite element approximation for the generalized displacements.

The present work is directed towards the development of a shell finite element for the impact response of multilayered shell panels.

References

[1] Noor AHK, Burton WS, Bert CW. Computational models for sandwich panels and shells. App Mech Rev 1996;49(3):155–99.

[2] Reddy J. Mechanics of laminated composite plates—Theory and analysis. Boca Raton: CRC Press; 1997.

[3] Sciuva MD. A third order triangular multilayered plate finite element with continuous interlaminar stresses. Int J Numer Meth Eng 1995;38:1–26.

[4] Carrera E. C^0 Reissner–Mindlin multilayered plate elements including zig-zag and interlaminar stress continuity. Int J Numer Meth Eng 1996;39:1797–820.

[5] Touratier M. An efficient standard plate theory. Int J Eng Sci 1991;29:901–16.

[6] Argyris J, Fried I, Scharpf D. The tuba family of plate elements for the matrix displacement method. Aero J R Aeronaut Soc 1968;72:701–9.

[7] Ganev H, Dimitrov T. Calculation of arch dams as a shell using an ibm-370 computer and curved finite elements. In: Theory of Shells. Amsterdam: North-Holland; 1980. p. 691–6.

[8] Béakou A, Touratier M. A rectangular finite element for analysing composite multilayered shallow shells in statics, vibration and buckling. Int J Numer Meth Eng 1993;36:627–53.

[9] Bernadou M. Finite Element Methods for Thin Shell Problems. New york: Wiley; 1996.

[10] Polit O, Touratier M, Lory P. A new eight-node quadrilateral shear-bending plate finite element. Int J Numer Meth Eng 1994;37:387–411.

[11] Srinivas S, Rao A. Bending, vibration and buckling of simply supported thick orthotropic rectangular plates and laminates. Int J Solids Struct 1970;6:1463–81.

[12] Pagano N. Exact solutions for rectangular bidirectional composites and sandwich plates. J Comp Mater 1970;4:20–34.